freshening. These trends over the past decade differ somewhat from previously reported multidecadal trends (Boyer et al. 2005; Hosoda et al. 2009; Durack and Wijffels 2010). These differences are not surprising given the different time periods over which the trends are computed.

The patterns of SSS differences of 2013 from 2012 derived from Aquarius data (Fig. 3.13b, colors) are reassuringly similar to those made from the Argo maps (Fig 3.11b, colors); however, in some locations the changes are visibly different in amplitude. The Argo differences also tend to have a bit more variance (on the scale of the Argo mapping and sampling scales) than do the Aquarius differences.

Maps from Aquarius data can be useful for examining the SSS seasonal cycle in detail (Fig. 3.13a); their agreement with Argo climatologies (e.g., Schmidtko et al. 2013) has improved between version 2.0 (e.g., Johnson et al. 2013b) and version 2.8.1 (Fig. 3.13a). Notably, version 2.8.1 exhibits high-latitude freshening from spring to fall that was not evident in version 2.0, and is now in better agreement with the seasonal cycle from Argo. Substantial freshening from March–May (MAM) to September–November (SON) is clear in the western Pacific fresh pool and under the ITCZ across the Pacific and Atlantic as tropical precipitation maxima shift with the seasons. Seasonal salinification just south of the equator in the Pacific is likely owing to mean Ekman advection acting on a seasonally varying salinity gradient (Yu 2011). There is strong salinification in the central tropical Indian Ocean between MAM and SON. Broadscale patterns of salinification between winter and summer in the eastern subtropics (Fig. 3.13a) in both hemispheres are typical of the seasonal cycle and most likely owing to entrainment of fresher water from below in the winter (Johnson et al. 2012b).

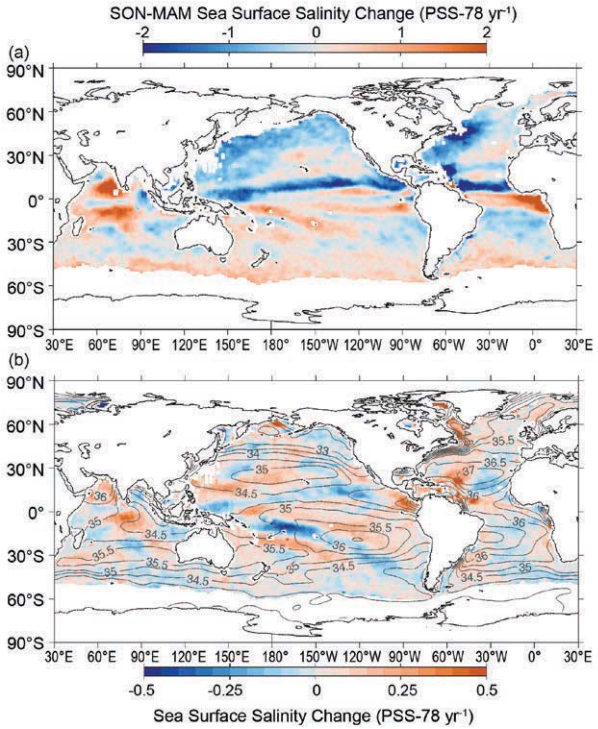

Fig. 3.13. Aquarius V2.8.1 SSS differences between (a) Sep–Nov and Mar–May 2013 monthly maps (colors in PSS-78), and (b) SSS differences of 2013 and 2012 from the means of differences of monthly maps (colors in PSS-78) with WOA 2009 values (yearly average of monthly maps, gray contours at 0.5 PSS-78 intervals) overlaid. White ocean areas have excessive land or ice contamination in the Aquarius field of view.

f. Subsurface salinity—T. Boyer, J. Antonov, J. Reagan, C. Schmid, and R. Locarnini

Evaporation minus precipitation ($E–P$) is well correlated with mixed layer salinity over much of the world's ocean (Yu 2011). It is difficult to accurately measure evaporation and precipitation over the ocean, so near-surface salinity can be used to constrain $E–P$ estimates (Schmitt 2008; Yu 2011). $E–P$ surface forcing has led to an intensification of the global hydrological cycle over the last 50 years, increasing salinity at the sea surface in areas dominated by evaporation and decreasing salinity in areas dominated by precipitation (Durack and Wijffels 2010; Durack et al. 2012). These surface changes are entrained into the subsurface ocean. Globally, near-surface salt content has increased in recent times compared to long-term averages, while intermediate waters have decreased in salinity (Roemmich and Gilson 2009; Helm et al. 2010). These changes are reflected in changes to ocean water mass composition and circulation patterns. Subsurface salinity changes, along with sea surface salinity (SSS) changes and ocean surface fluxes are important for understanding changes to the ocean and in the atmosphere, both of which affect the global climate system.

To investigate changes to subsurface salinity, all available subsurface salinity profile data for 2013 were used to derive 1° average gridded salinity anomalies at standard depths from the surface to 2000 m. The anomalies were calculated as differences from the 1955–2006 average (Antonov et al. 2010). Differences from recalculated salinity anomaly fields for 2012 are also used to investigate year-to-year variations in salinity. A full description of the method can be found in Boyer et al. (2012).

At present, the single largest source of salinity profiles for the world's ocean is the Argo program with its fleet of profiling floats (Roemmich et al. 2009). From this program, 144 463 salinity profiles were used in the process of calculating subsurface salinity anomalies for 2013. About two-thirds of all float profiles reach 2000 decibars. Because it takes a minimum of six months of data to calculate a final adjustment for salinity drift, less than 10% of the profiles are of the higher level quality-controlled delayed-mode data. For this reason, real-time salinity data with basic quality control were also utilized in this study. Of these, 80 952 profiles include salinity drift adjustments calculated for earlier cycles in a floats lifetime.

In addition to the Argo data, another major source of salinity data is 27 743 daily average profiles from tropical moored buoys (http://www.pmel.noaa.gov/tao/). Included are data from the TAO/TRITON array in the Pacific, PIRATA in the Atlantic, and RAMA in the Indian Ocean, where the deepest measurement was usually at 500-m depth. Almost all buoys are located within 10° latitude of the equator. There also were 14 143 CTD casts largely concentrated in the northwest Pacific and northwest Atlantic and 20 320 profiles from gliders (localized mostly in the Gulf of Mexico, far western Pacific, and northeast Atlantic), most of which were made available through the Global Temperature and Salinity Profile Project (GTSPP). In order to examine the year-to-year change in salinity, anomaly fields for 2012 were recalculated based on updated quality control provided by Argo. A total of 48 558 of the 133 518 Argo salinity profiles recorded in 2012 that were used in this study have now been delayed-mode quality controlled. All salinity and salinity anomaly data were examined using quality control procedures outlined in Boyer et al. (2013a) and are available through the World Ocean Database (Boyer et al. 2013a). All derived fields can be found at http://www.nodc.noaa.gov/OC5/3M_HEAT_CONTENT/. Average salinity anomalies for the upper 100 m at each 1° grid were also computed. The geographic distribution of these fields is similar to SSS fields as presented in section 3e.

The zonally-averaged difference between salinities in the Pacific Ocean in 2013 and the long-term average are shown in Fig. 3.14a. The zonally averaged differences >±0.1 (blue and red shaded areas) in Fig. 3.14a, and subsequent figures, are significant at the 5% confidence level based on Student T tests. Much of the South Pacific was fresher than average in 2013, with the exception of the upper 250 m in the subtropics and along the equator. Below the higher salinity area in the subtropics, freshening was stronger in 2013 than in 2012. Between 50°S and 40°S a freshening relative to average was observed even at depths exceeding 1500 m. Meijers et al. (2011) attribute the freshening in this region to southward movement of the Antarctic Circumpolar Current and water mass changes possibly due to increased precipitation and ice melt. Farther south along the 34.6 isohaline, higher salinity relative to the long-term mean was found. The 2013 salinity anomalies in the South Pacific are comparable to the 2012 salinity anomalies (Boyer et al. 2013b), but with increased salinities reaching deeper in many areas. For example, the area of high salinity south of 50°S in 2013 (Fig. 3.14b) extends to depths greater than 750 m along the 34.6 isohaline near 60°S. Salinity in the upper 100 m (see Fig. 3.11a) shows a large positive salinity anomaly relative to the average under the South Pacific convergence zone (SPCZ), sloping from near the equator in the far western Pacific to around 30°S in the eastern Pacific, similar to 2011 (Johnson et al. 2013b), whereas this feature was weaker in 2012 (see Fig. 3.11b). In the North Pacific, as for 2012, 2013 differed from average with saltier conditions in the upper 250 m near the equator. Freshening at midlatitudes down to 750-m depth, is consistent with the thermocline freshening described by Ren and Riser (2010). Salinity increase exceeding 0.02 occurred in 2013 relative to 2012 below 250 m north of 40°N in the Pacific, including the Bering Sea area. In fact, 2013 salinity in the Bering Sea was similar to 2011 with higher salinity relative

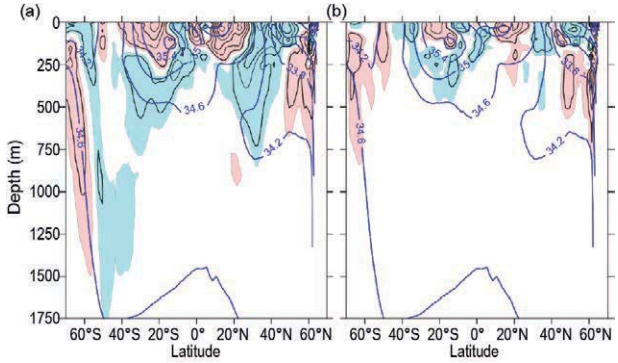

Fig. 3.14. Zonally-averaged (a) 2013 salinity anomaly and (b) 2013 minus 2012 salinity field for the Pacific Ocean. For both figures, blue shading represents negative (fresh) anomalies <-0.01, red shading represents positive (salty) anomalies >0.01. The contour interval for the anomalies is 0.02. In the background of each figure (thick blue contours) is the zonally averaged climatological mean salinity (WOA09). Contour intervals for the background are 0.4. All values are PSS-78 .

to the long-term trend, while a freshening was seen in this area in 2012.

Between the mid-1950s and the mid-1990s an increase in salinity in the subtropical and tropical North Atlantic was coupled with a decrease in salinity in the subpolar North Atlantic (Curry et al. 2003; Boyer et al. 2007; Wang et al. 2010). Since the mid-1990s, both the subtropical and subpolar North Atlantic exhibit increased salinity (Boyer et al. 2007; Wang et al. 2010). This pattern persisted into 2013 (Fig. 3.15a), with the exception of a freshening around 50°N. Most of the North Atlantic increased in salinity in 2013 compared to 2012 in the upper 100 m, with substantial freshening (>0.02) in 100–500-m depth primarily north of about 30°N, in contrast to 2012 where there was freshening over 2011 from the surface to 750-m depth (Fig. 3.15b). Freshening >0.02 extends deeper than 500-m depth around 30°N. This area of freshening expands at shallower depths, with its maximum extent at 150-m depth between 15° and 40°N. At shallower depths, the tropical and subtropical regions of the North Atlantic experienced a large increase in salinity (>0.06). It may be that the freshening signal in the North Atlantic in 2012 was a short-lived anomaly in the decadal signal of increased salinity in the subpolar and subtropical North Atlantic. In contrast to the North Atlantic, the South Atlantic salinity signal in 2013 indicates that the long-term trend was strengthened when compared with the anomalies for 2012. Positive salinity anomalies exceeding 0.06 were found for 2013 down to 250-m depth from 5°–25°S, with anomalies exceeding 0.02 below 500 m south of 20°S. South of 40°S in the Atlantic Ocean, a deep freshening is observed, to depths below 750 m, shoaling to the south, where the freshening is limited to the upper 100-m depth. Between 2012 and 2013, the positive salinity anomalies weakened in the upper 150 m between the equator and 40°S, whereas they strengthened below 150-m depth (Fig. 3.15b). South of 40°S, the trends between 2012 and 2013 were strengthened.

In the Indian Ocean, the differences between 2013 salinity zonal means and the long-term average (Fig. 3.16a) include deep (>1000-m depth) freshening south of the equator, interrupted by increased salinity in the midlatitude south Indian Ocean from the surface narrowing to a maximum depth of 800 m at 40°S. In the upper 100 m (see Fig. 3.11a), the salty anomaly at latitudes north of 30°S is confined to the western half of the Indian Ocean, with freshening in the eastern Indian Ocean. South of 30°S, the positive anomaly extends across the entire basin in a narrow band north of 50°S. The salinity change from 2012 to 2013 in the south Indian Ocean was small (<0.02; Fig. 3.16b), except south of 60°S, where there were limited observations, and just south of the equator in the upper 100 m. Most of the North Indian Ocean zonally-averaged anomalies for 2013 continue to be salty down to depths exceeding 700 m. From 2012 to 2013, changes in the north Indian Ocean larger than 0.02 were mainly confined to the upper 150-m depth and are of the opposite sign when compared with the changes from 2011 to 2012. The fresh anomaly in the upper 100-m depth (see Fig. 3.11b) is less than 0.02 in the central equatorial Indian Ocean, which is smaller than the salty anomaly in the western equatorial Indian. This is the opposite pattern as found between 2011 and 2012. There was a positive Indian Ocean dipole (IOD, east-west temperature gradient >0.5°C) in both 2011 and 2012, but a negative IOD in 2013. It is unclear if there is any relation between the IOD and the upper 100-m average salinity anomaly. In the northern reaches of the Indian Ocean, following the same pattern seen between 2011 and 2012, the eastern Arabian Sea was saltier in 2013 than 2012, while the western Arabian Sea was fresher. Opposite to the

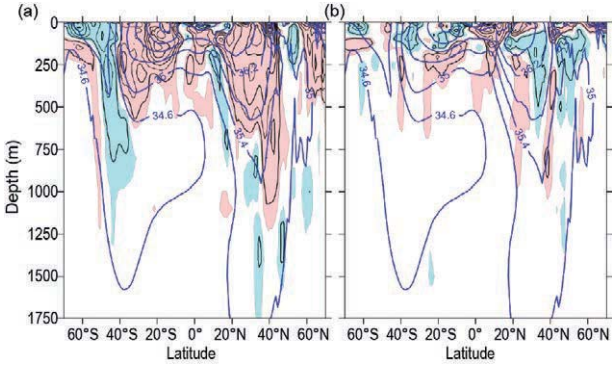

Fig. 3.15. Zonally-averaged (a) 2013 salinity anomaly and (b) 2013 minus 2012 salinity field for the Atlantic Ocean.

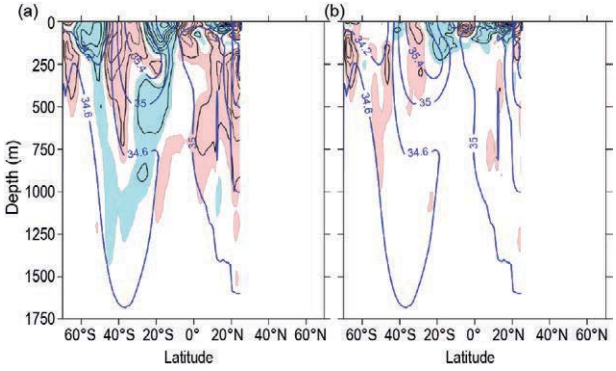

Fig. 3.16. Zonally-averaged (a) 2013 salinity anomaly and (b) 2013 minus 2012 salinity field for the Indian Ocean.

pattern between 2011 and 2012, the northeast Bay of Bengal was saltier in 2013 than 2012, while the rest of the Bay of Bengal was fresher in 2013 than in 2012.

g. Surface currents—R. Lumpkin, G. Goni, and K. Dohan

This section describes ocean surface current changes, transports derived from ocean surface currents, and features such as rings inferred from surface currents. Surface currents are obtained from in situ (global array of drogued drifters and moorings) and satellite (altimetry, wind stress, and SST) observations. Transports are derived from a combination of sea height anomaly (from altimetry) and climatological hydrography. See previous *State of the Climate* reports, from 2011 and before, for details of these calculations. Anomalies are calculated with respect to the time period 1992–2007. Global zonal current anomalies and changes in anomalies from 2012 are shown in Fig. 3.17 and discussed below for individual ocean basins.

1) Pacific Ocean

Compared to the dramatic changes in 2012, 2013 was a relatively quiescent year in the tropical Pacific basin. It began with average January westward surface current anomalies of –25 to –30 cm s^{-1} (negative = westward) across the equatorial Pacific in the band 170°E–90°W, where the climatological westward speed is ~65 cm s^{-1}. By February, these equatorial anomalies had diminished dramatically and were present only in the longitude band 90°–150°W. Throughout the remainder of 2013, no large-scale equatorial anomalies persisted for more than a month.

The eastward North Equatorial Countercurrent (NECC) at 5°–8°N was ~10–20 cm s^{-1} faster than its climatological average from January until August. The longitude of anomalously fast NECC currents shifted westward through these months, located at 90°–140°W in January, 130°–160°W in June, and 130°W–180° in August. These anomalies weakened in September–October, and in November the NECC was close to its climatological strength across the basin.

In March, strong eastward anomalies of 20–30 cm s^{-1} developed at 2°S along 100°–150°W, where the climatological currents are near zero. The location of the anomalies propagated westward and diminished in magnitude through May, located at 150°W–180° in May when they were last seen.

The annual-average zonal current anomaly for 2013 in the Pacific (Fig. 3.17a) highlights the NECC anomalies at 5°–8°N that persisted through most of the year west of the dateline (see above). In the band 145°–170°E, anomalies of 15 cm s^{-1} at 20°N indicated a strengthening of the eastward Subtropical Countercurrent, while anomalies of –15 cm s^{-1} at 22°N corresponded to a strengthening of the westward flow located at this latitude. Alternating zonal bands of ~20 cm s^{-1} anomalies at 33°–36°N, 140°–160°E were consistent with a northward shift of the Kuroshio Extension from its annual climatological position, a shift seen since 2010. For the period 2010–13, the Kuroshio has exhibited a narrower and stronger annual mean signature, shifted approximately 1° in latitude to the north compared to 2006–09. While the climatological latitude of the Kuroshio core at 150°E is ~34.3°N, the core of the current in 2013 was at ~36.0°N, slightly south of the mean position during 2012 (36.7°N). The 2013 minus 2012 map (Fig. 3.17b) is dominated by the strong eastward anomalies that were present in February–August 2012 (Lumpkin et al. 2013).

Surface current anomalies in the equatorial Pacific typically lead SST anomalies by several months, with a magnitude that scales with the SST anomaly magnitude. Recovery to normal current conditions is also typically seen before SST returns to normal. Thus, current anomalies in this region are a valuable predictor of the evolution of SST anomalies and their related climate impacts. This leading nature can

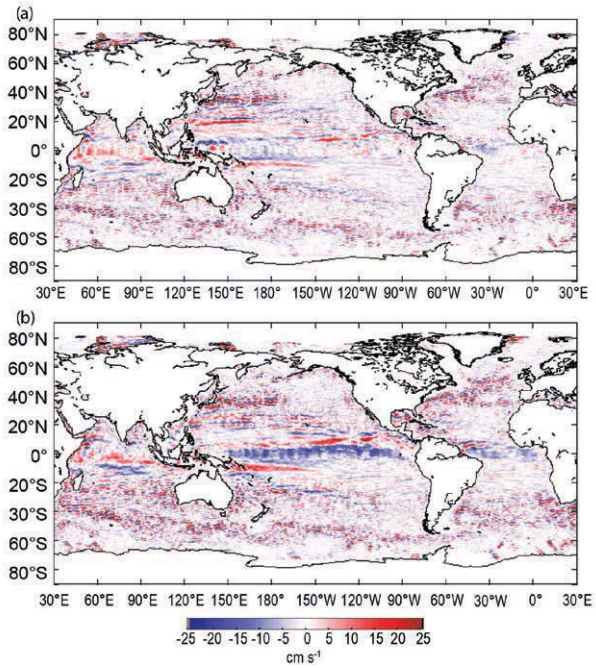

Fig. 3.17. Global zonal geostrophic anomalies for (a) 2013 and (b) 2013 minus 2012, in cm s^{-1}, derived from a synthesis of drifters, altimetry, and winds.